




# Acai Residue as an Ecologic Filler to Reinforcement of Natural Rubber Biocomposites

Samara S. Araújo<sup>a</sup>, Gleyson T. A. Santos<sup>b</sup>, Gabrieli R. Tolosa<sup>b</sup>, Carlos T. Hiranobe<sup>a</sup> ,  
Eduardo R. Budemberg<sup>a</sup>, Flávio C. Cabrera<sup>a</sup>, Michael J. da Silva<sup>a</sup> , Leonardo L. Paim<sup>a</sup>,  
Aldo E. Job<sup>b</sup>, Renivaldo J. dos Santos<sup>a\*</sup> 

<sup>a</sup>Universidade Estadual Paulista (UNESP), Faculdade de Engenharia e Ciências, Departamento de Engenharia, Avenida dos Barrageiros, 1881, 19274-000, Rosana, SP, Brasil.

<sup>b</sup>Universidade Estadual Paulista (UNESP), Faculdade de Ciências e Tecnologia, Departamento de Física, Rua Roberto Simonsen, 305, 19060-900, Presidente Prudente, SP, Brasil.

Received: November 28, 2022; Revised: March 23, 2023; Accepted: May 03, 2023

The biodiversity of plant resources is a renewable source that can use as a sustainable component in various applications. The use of vegetable waste as a filler element in polymeric composites is part of the solid waste management policy and the sustainable development of agribusiness. In this work, the natural rubber composites were prepared with acai seed in proportions of 0, 10, 20, 30, 40, and 50 phr (per hundred rubber). The composites were homogenized in an open cylinder mixer and characterized by rheometric, morphological, mechanical, and thermal tests. The addition of the organic fillers significantly reduced the vulcanization process time. Thermogravimetric analysis and infrared spectroscopy showed that the composites were thermally stable and showed no structure changes after the vulcanization process, respectively. The Lorenz-Parks method's evaluation of matrix/filler interactions showed a strong interaction between NR/Acai. The new biocomposite can replace non-ecological composites economically and sustainably.

**Keywords:** *Acai, biocomposites, Lorenz-Parks, Mooney-Rivlin, vulcanization, sustainability.*

## 1. Introduction

The acai (*Euterpe oleracea* Mart.) is one of the most important fruits of plant extraction in the Amazon region and the consumption of its pulp has increased more and more in the national and international markets<sup>1</sup>. In 2020, 220 thousand tons of acai fruit were produced, with Pará being the largest producer in the Brazilian state<sup>2</sup>. However, only 20% of the fruit is used in the form of pulp by the food<sup>3</sup>, pharmaceutical<sup>1</sup>, biomedical<sup>4</sup>, and cosmetics<sup>5</sup> industries, so approximately 176 thousand tons are waste discarded in landfills by the agroindustry<sup>6</sup>.

The pulpless acai seed consists of the inedible part of the fruit that comprises the extractives (fats, lipids, resins, steroids, tannins, terpenes, terpenoids, phenolic compounds, and flavonoids) and three building blocks, hemicellulose, cellulose and lignin<sup>4</sup>. Lignocellulosic biomass is a promising, sustainable, and economical alternative as a raw material in the cement industry<sup>5</sup>, energy conversion<sup>4</sup>, and ecological composites<sup>3</sup>. The development of new composite materials based on natural fibers is on the rise as sustainable building materials in most developing countries<sup>7</sup>. Its application aims to strengthen the microstructure of the material, increasing the tensile strength, heat, and the interaction between filler/matrix, reducing the effects of cracking and matrix degradation<sup>8</sup>.

Recently, research has been conducted using lignocellulosic fibers from the biomass of acai residue. Tavares et al.<sup>9</sup>, investigated the effect of heat treatment in autoclave on chemical, physical and morphological properties of lignocellulosic fibers of acai (*Euterpe oleracea* Mart), and the behavior of this treated fiber in composites of polypropylene (PP) matrix with polypropylene-graft-maleic anhydride (PPgMA) as coupling agent. Oliveira et al.<sup>6</sup>, evaluated the changes in density, chemical structure, morphology, water absorption, porosity, and thermal and mechanical properties in castor bean-based polyurethane reinforced with acai residue (5-20% by weight). Barbosa et al.<sup>2</sup>, evaluated the performance of acai residue as reinforcement in agglomerated panels and made the panels considering two factors: granulometry and different fractions of resin. Lima et al.<sup>1</sup>, analyzed the potential of the residual biomass of acai in biotechnological applications, such as fermentation processes and the production of fermentable sugars (mannose) for food and pharmaceutical purposes, for this, they characterized the samples in different states of maturity. Azevedo et al.<sup>5</sup>, investigated the effect of incorporating ground acai fibers (in natural and chemically treated with NaOH and HCl) in replacement of 5-10% by weight of Portland cement on rheology, hydration, and microstructure of pastes. Martins et al.<sup>3</sup>, used acai fibers to obtain composites with natural rubber from different types of clones. In the past, natural rubber latices from different clones

\*e-mail: [renivaldo.santos@unesp.br](mailto:renivaldo.santos@unesp.br)

of *Hevea brasiliensis* were evaluated for the incorporation of acai residues<sup>3</sup>, however, the tensile strength was decreased by increasing the amount of acai by 5 and 10% and without influence over thermal properties.

Here, we evaluated the acai waste biomass as filler for mechanical reinforcement of natural rubber composites evaluated by stress-strain mechanical tests. Also, we used the Lorenz-Parks equation correlated with the crosslink density by the Flory-Rehner method to determine the interfacial interaction between the filler and the matrix and compared it with the results obtained by the Mooney-Rivlin method, allowing thus, understanding the behavior of the interaction between the acai fibers and the polymer matrix.

## 2. Material and Methods

### 2.1. Material

The natural rubber (NR) used was the Brazilian clear crepe type (BCC) and was purchased from DLP “*Indústria e Comércio de Borracha e Artefatos LTDA*” (São Paulo, Brazil). The acai residue was collected at Fazenda Marajeri, located in the Amazon region (Pará, Brazil). The acai seeds were exposed to the sun for a period of 12 hours to dry excess moisture. Then, they were micronized in a knife mill, sieved to a granulometry of 30 mesh and placed in

an oven at 104 °C for 24 h. Vulcanization reagents such as zinc oxide, stearic acid, polyethylene glycol (PEG 4000), processing oil, antioxidant, sulfur, and accelerators of 2-mercaptobenzothiazole disulfide (MBTS), and tetramethyl thiuram disulfide (TMTD), were purchased commercially.

#### 2.1.1. Preparation of composites

Table 1 presents the formulation for the preparation of NR/Acai composites.

Compounds were prepared in two rolls mill with a friction ratio of 1:1.25 according to ASTM D3182<sup>10</sup> in proportions of 0, 10, 20, 30, 40, and 50 phr. In the first stage, natural rubber, reaction activators (zinc oxide and stearic acid), plasticizers (polyethylene glycol 4000 and naphthenic oil), antioxidant (vulcanox), and micronized acai residue were added to the mixer. After homogenization of the mixture, the mass was allowed to rest for 24 h at a room temperature of 23 °C. In the second step, the mass was reinserted into the mixer to add the crosslinking agent (sulfur) and vulcanization accelerators (MBTS and TMTD). After the second mixture homogenization, the mass was allowed to rest for more than 4 h at room temperature. After completing the steps, the rheometric tests were carried out from specimens made in thermos-press. Figure 1 shows the raw materials and equipment used in the composites production process.

**Table 1.** Formulation of natural rubber and acai composites.

Phases of process	Components	Quantities of components in phr*					
		NR/A <sub>0</sub>	NR/A <sub>10</sub>	NR/A <sub>20</sub>	NR/A <sub>30</sub>	NR/A <sub>40</sub>	NR/A <sub>50</sub>
1 <sup>st</sup> . Stage Activation	NR (CCB)	100	100	100	100	100	100
	Zinc oxide	5	5	5	5	5	5
	Stearic acid	2	2	2	2	2	2
	PEG 4000	0	2	2	2	2	2
	Vulcanox	0	1.5	1.5	1.5	1.5	1.5
	Naphthenic oil	0	10	10	10	10	10
	Acai residue	<b>0</b>	<b>10</b>	<b>20</b>	<b>30</b>	<b>40</b>	<b>50</b>
2 <sup>nd</sup> . Stage Acceleration	Sulfur	1.5	1.5	1.5	1.5	1.5	1.5
	MBTS	1	1	1	1	1	1
	TMTD	0.5	0.5	0.5	0.5	0.5	0.5

\*phr (per hundred rubber). NR/A (composite of natural rubber and acai).

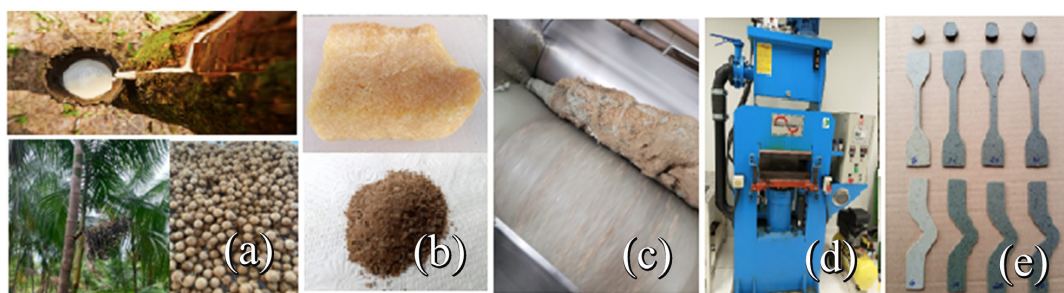


**Figure 1.** Raw material used: a) Rubber tree (latex) and acai seed; b) Natural rubber and micronized acai; c) and incorporation of acai residue in the rubber; d) Vulcanization in hydraulic thermopress; e) specimens.

## 2.2. Methods

### 2.2.1. Rheological properties

The rheometric parameters were obtained from an oscillatory disk rheometer of the brand Team Equipamentos. The tests were carried out according to ASTM D2084-19a<sup>11</sup>, in which the composite was subjected to an arc of oscillation of 1° and isotherms of 150 °C. With the rheometric parameters measured, the NR and acai compounds were submitted to the thermo-pressing process, using the Mastermac-Modelo Vulcan 400/20-1 press, with a maximum pressure of 210 kgf cm<sup>-2</sup> and aid of a 1010/1020 steel mold (150 x 150 x 2 mm).

### 2.2.2. Density

The determination of the density of the composites was obtained according to ASTM D297<sup>12</sup> using ethyl alcohol with a density of 0.79 g cm<sup>-3</sup> and calculated by Equation 1:

$$\rho = \frac{\rho_L * m_A}{m_A - m_B} \quad (1)$$

Where  $\rho$  is the density of the sample (g cm<sup>-3</sup>);  $\rho_L$  represents the density of ethanol at the analysis temperature (g cm<sup>-3</sup>);  $m_A$  is the mass of the wireless sample in the air (g) and the  $m_B$  is the mass of the wireless sample in the liquid (g).

### 2.2.3. Cross-link density by the swelling method – Flory-Rehner

The crosslink density of the composites was calculated using the swelling technique. The specimens were weighed with a mass of approximately 0.25 ± 0.05 g and immersed in toluene for 5 days. Then, the samples were removed, dried at room temperature to remove excess solvent, weighed, dried in an oven at 80 °C for 24 h, and weighed again to obtain samples without solvent. The resulting values of the mass of the dry specimen, the mass of the specimen swollen with solvent, and the mass of the specimen after swelling were recorded and used to estimate the volumetric fraction of rubber in the swollen specimen. Thus, the crosslink density was calculated using the following Equation 2 developed by Flory and Rehner<sup>13</sup>. The values used for the molar volume of toluene ( $V_0$ ) and the Flory-Huggins interaction parameter ( $\chi$ ) for natural rubber and toluol were 106.3 cm<sup>3</sup> mole<sup>-1</sup> and 0.393, respectively.

$$v = \frac{-\ln(1 - V_B) + V_B + \chi(V_B)^2}{(\rho_B)(V_0) \left( V_B^{\frac{1}{3}} - \frac{V_B}{2} \right)} \quad (2)$$

Where  $v$  is the cross-link density (mol cm<sup>-3</sup>);  $\rho_B$  is the density of the rubber (g cm<sup>-3</sup>) and  $V_B$  is the volume fraction of rubber in the swollen form, determined from the swelling weight gain.

### 2.2.4. Cross-link density by tensile test – Mooney-Rivlin

Crosslink densities were also estimated by the Mooney-Rivlin method<sup>14</sup> based on tensile strength tests. The semi-empirical Equation 3<sup>15</sup> was used to plot the graph in the linear region to obtain the network parameters.

$$\sigma = \frac{F}{2A_0(\lambda - \lambda^{-2})} = C_1 + \frac{1}{\lambda} C_2 \quad (3)$$

Where  $F$  is the force required in the vulcanized material;  $A_0$  is the cross-sectional area (mm<sup>2</sup>);  $\lambda$  is the rate of extension ( $1 + \epsilon$ ), where  $\epsilon$  is the strain;  $C_1$  and  $C_2$  are constants of material, while  $C_1$  is assumed to be the contribution of the crosslinking units,  $C_2$  is the Mooney-Rivlin elastic constant and considered as the contribution of trapped tangles.

The material constant  $C_1$  can be used to calculate the crosslink densities through Equation 4<sup>16</sup>

$$\eta = \frac{C_1}{RT} \quad (4)$$

Where  $\eta$  is the cross-link density (mol cm<sup>-3</sup>);  $R$  is the universal gas constant and  $T$  is the absolute temperature (K).

### 2.2.5. Scanning electron microscopy (SEM) and energy dispersive X-rays (EDX)

The surface morphology of the fractured composites was investigated in a Carl Zeiss EVO LS15 scanning electron microscope at 20 kV. The samples were coated with a thin layer of gold using a Quorum Q 150R ES sputter coater. The chemical elements present at a certain point in the material were identified by EDX (energy dispersive X-rays).

### 2.2.6. Acai X-ray fluorescence

The chemical composition of the samples was determined by means of the X-ray fluorescence assay performed on the analytical spectrometer, Axios series, model PW 4400/40. The results were obtained from SUPERQ 5.1B software, Om application. The fluorescence assay qualitatively and quantitatively determines the elemental composition of the samples, i.e., it is possible to identify the elements and their respective amounts present in the samples.

### 2.2.7. Elemental organic analysis of acai

The elemental compositions of the samples were determined from 2 to 3 mg of dry sample, in triplicate, using the elemental analyzer brand Thermo Scientific, model Flash AE 1112. The basic operating principle of this equipment is the separation of gases formed in the form of CO<sub>2</sub>, N<sub>2</sub>, H<sub>2</sub>O, and H<sub>2</sub>SO<sub>3</sub>, which are transported by helium gas in a column and detected by thermal conductivity. The contents of carbon (C), hydrogen (H), nitrogen (N) and sulfur (S), and oxygen (O) were determined.

### 2.2.8. Fourier transform infrared spectroscopy (FTIR)

FTIR spectroscopy was performed using a Bruker Vector 22 spectrometer in ATR mode (attenuated total reflection) in the range of 4000-400 cm<sup>-1</sup> with a spectral resolution of 4 cm<sup>-1</sup> and 32 scans.

### 2.2.9. Tensile strength test and accelerated aging test

The tensile tests were performed on the Instron/Emic DL2000 universal testing machine at 500 mm min<sup>-1</sup> with a load cell of 5 kN and a transducer of internal deformation. For these tests, quintuplicates of specimens of type A (bodies

of straight section and dumbbell) were used, according to the ASTM D412 standard<sup>17</sup>.

The aging process was carried out in accordance with ASTM D573<sup>18</sup>, in which the specimen is placed in a circulating air oven for 70 hours at a temperature of 70 °C.

### 2.2.10. Shore A hardness

Hardness determination was performed on the surface of the composites according to ASTM D2240<sup>19</sup> on the Shore A scale, using a Digimess brand analog durometer with a capacity of 0 to 100 and grading 1 Shore A. The analysis was performed in triplicate.

### 2.2.11. Loss from abrasion

Abrasion loss was calculated using Equation 5, according to ASTM D5963<sup>20</sup>, using MaqTest brand equipment with an abrasion stroke equivalent to 40 m and pressure in the specimen on the cylinder of 5 N.

$$PA = \frac{\Delta m S_0}{\rho S} \quad (5)$$

Where PA represents the abrasion loss ( $\text{mm}^3 \text{40 m}^{-1}$ );  $\Delta m$  is the composite mass loss (mg);  $S_0$  is the theoretical attack index of sandpaper on standard rubber ( $200 \pm 20 \text{ mg}$ );  $S$  is the actual etching index of the sandpaper on standard rubber (mg) and  $\rho$  is the density of the composite ( $\text{mg mm}^{-3}$ ).

### 2.2.12. Analysis of interactions between natural rubber and micronized acai residue using the Lorenz-Parks equation

The interaction between the acai residue powder and the natural rubber was determined by the method developed by Lorenz and Park<sup>21</sup> and the parameters obtained from the swelling tests in the solvent used Equation 6<sup>22</sup>:

$$\frac{Q_f}{Q_g} = ae^{-z} + b \quad (6)$$

Where  $Q$  is the weight of toluene absorbed per gram of rubber, the subscripts  $f$  and  $g$  represent the vulcanized composite with filler and gum, respectively;  $z$  is the ratio of the mass of the filler per unit mass of rubber, and  $a$  and  $b$  are the constants. The value of  $Q$  is calculated using Equation 7:

$$Q = \frac{w_s - w_d}{w_r \cdot x100 / w_F} \quad (7)$$

Where  $w_s$  is the weight of the swollen composite when equilibrium is reached;  $w_d$  is the dry composite weight;  $w_r$  is the weight of rubber in the dry composite and  $w_F$  is the total weight of the formulation.

### 2.2.13. Thermogravimetric Analysis (TG)

The Thermogravimetric Analysis (TG) tests were carried out in a NETZSCH model 209 equipment, with an ambient temperature range from around 25 °C to 900 °C, with a heating rate of 10 °C  $\text{min}^{-1}$  in the atmosphere of nitrogen and flow of 15 mL  $\text{min}^{-1}$ . The amount of mass used to perform the measurements was approximately 10 mg, according to ASTM D6370<sup>23</sup>.

## 3. Results and Discussion

### 3.1. Analysis of rheometric parameters

The values of rheometric parameters, such as minimum torque ( $M_L$ ), maximum torque ( $M_H$ ), torque variation ( $\Delta M$ ), pre-cure time ( $t_{s1}$ ), and optimal curing time ( $t_{90}$ ) are shown in Table 2.

Table 2 shows the values of the minimum torques of the composites. The data showed that there is a small gradual variation of the values due to the increase in viscosity due to the reduction in the mobility of the macromolecular chain of rubber with the dispersion of the fillers in the polymer matrix. The maximum torque is related to the formation of the cross-links and the presence of fillers, it is noted that the  $M_H$  also increased gradually with the addition of the fillers. The incorporation of fillers also increased the torque variation that is related to the processability of the composite after the formation of the cross-links and the interactions with the filler. The  $t_{s1}$  and  $t_{90}$  decreased considerably compared to the composite without fillers, this fact may be related to the constituent of acai identified in the analysis of X-ray fluorescence, such as alkali metals that enhance the action of accelerators (potassium, calcium, and rubidium), zinc was used as an activation agent in the vulcanization process and the presence of fatty acids, identified by Melo et al.<sup>24</sup>.

### 3.2. Analysis of scanning electron microscopy and energy dispersive X-ray spectroscopy

Figure 2 presents photos and images obtained from Scanning Electron Microscopy (SEM). In Figure 2a was observed that the acai seed is composed of the mesocarpic

**Table 2.** Rheometric parameters of NR/Acai composites.

Composites	$M_L$	$M_H$	$\Delta M = (M_H - M_L)$	$t_{s1}$	$t_{90}$
NR/Acai	(dNm)	(dNm)	(dNm)	(min)	(min)
0 phr	1.40 ± 0.06	20.43 ± 0.61	19.03 ± 0.62	4.98 ± 0.09	7.00 ± 0.46
10 ph	1.53 ± 0.07	24.01 ± 1.25	22.48 ± 1.28	1.81 ± 0.04	2.73 ± 0.31
20 phr	1.95 ± 0.06	26.47 ± 1.27	24.52 ± 1.28	1.74 ± 0.03	2.66 ± 0.31
30 ph	1.98 ± 0.11	29.12 ± 1.38	27.14 ± 1.34	1.67 ± 0.04	2.53 ± 0.30
40 phr	2.03 ± 0.16	31.13 ± 0.94	29.09 ± 0.87	1.65 ± 0.05	2.51 ± 0.23
50 phr	2.37 ± 0.18	34.83 ± 1.27	32.46 ± 1.11	1.64 ± 0.03	2.48 ± 0.16

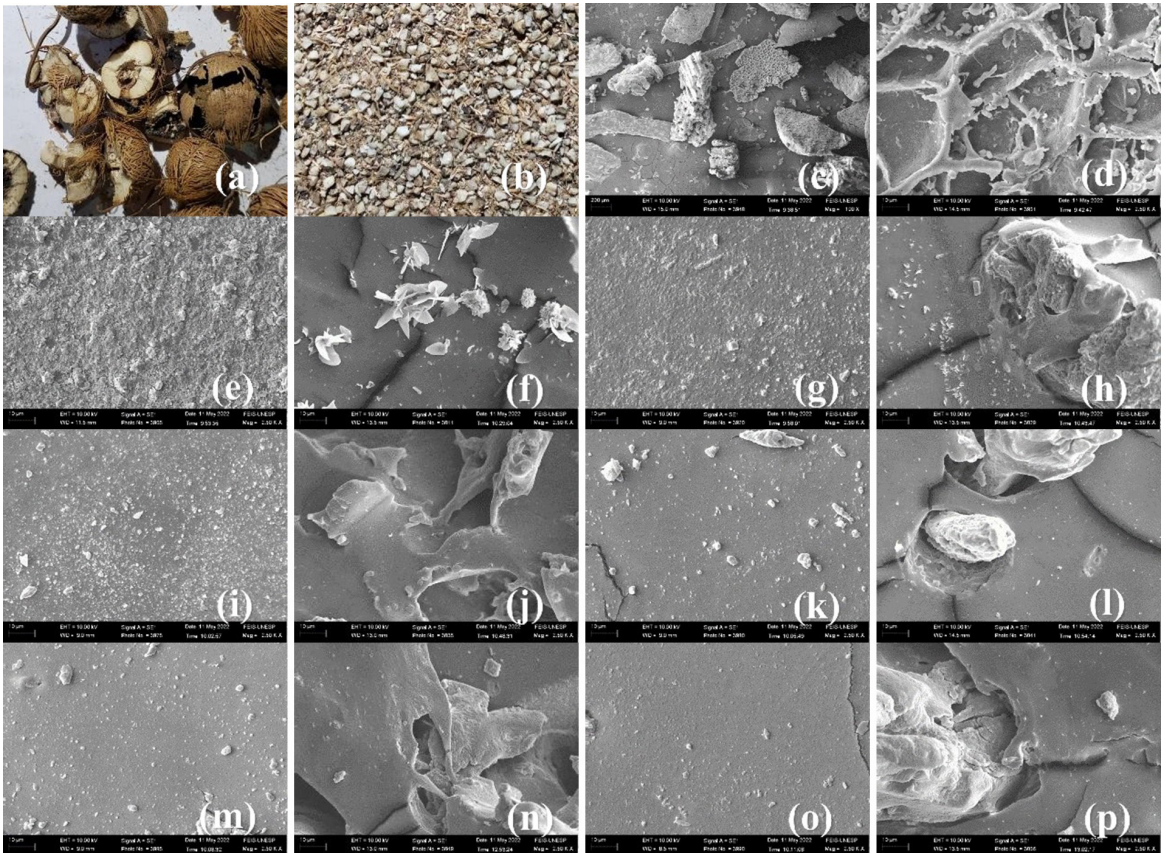
fibers, which is the outer part of the acai berry, and the endocarp, which is the whitish inner part of the seed. After the micronization process on a 30-mesh sieve, Figure 2b shows that the samples are composed of fibers and granular particles. Figure 2c is a 100 times magnification of the acai particles where it is possible to notice, on the surfaces of the granules, the porosities, and their geometric irregularities. Figure 2d is a 2500 times magnification in which we observe the structure of the lignocellulosic surface in hexagonal shape and some fibers scattered throughout the biomass structure.

Figure 2e to 2p are from the BN/Acai composites from the specimens used in the tensile strength tests. Figure 2e refers to the rough surface of the composite without the filler (reference sample). The surface becomes smoother and more homogeneous as larger amounts of filler are incorporated (10, 20, 30, 40, and 50 phr), as observed in Figure 2g, 2i, 2k, 2m, and 2o. Figure 2f refers to the cross-sectional area (fracture) of the unfilled compound and shows the presence of cracks and outcropping of reagents. Figure 2h, 2j, 2l, 2n, and 2p show the fracture images of the fillers encapsulated in the elastomeric matrix, there is a good interaction between the matrix and fillers, in addition, the addition of fillers reduced crack propagation and this fact

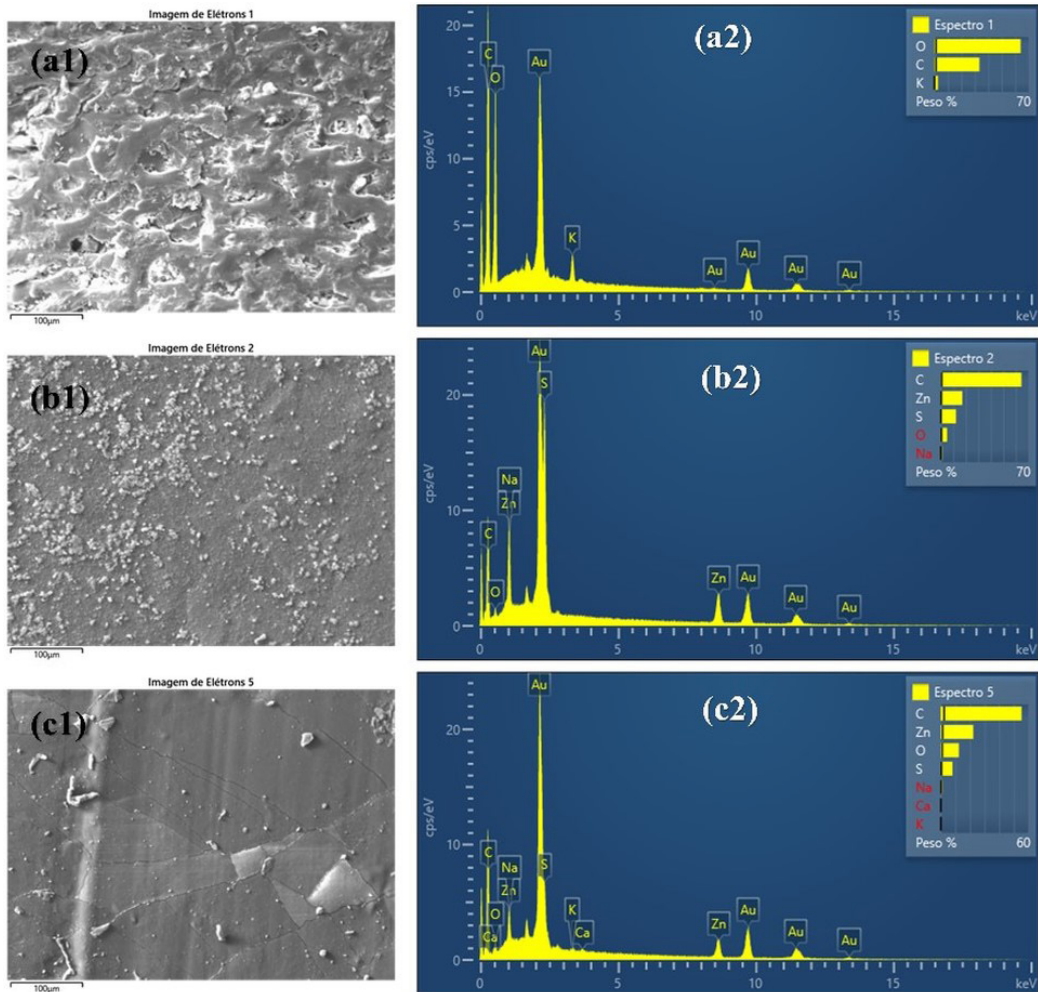
may be related to the degree of reinforcement that the filler offers in synergy with the matrix.

Figure 3 shows the scanning electron microscopy (SEM) images of the surface area of the samples where the test areas were submitted to energy dispersive spectroscopy (EDX) to identify the chemical elements that make up the samples.

Figure 3a1 refers to the micronized acai residue, and Figure 3a2 identifies the amount of each acai constituent: 33.32% carbon, 64.07% oxygen, and 2.61% potassium. In Figure 3b1 we observe the test area of the unfilled composite and in Figure 3b2 we can see that the unfilled composite has: 64.41% carbon, 5.08% oxygen, 1.15% sodium, 12.11% sulfur, and 17.25% zinc, the presence of the chemical element carbon is due to the chemical structure isoprene of natural rubber, other chemical elements detected in the EDX are related to the chemical additives added in the vulcanization process, such as sulfur which is a cross-linking agent, zinc from zinc oxide which is an activating agent and sodium which is probably the constituent element of the processing oil. Figure 3c1 refers to the surface area of the composite with 30 phr and Figure 3c2 of the NR/Acai composite identified the presence of all constituents of the acai residue and natural rubber mentioned above, in addition to presenting 0.40% calcium, probably from the filler.



**Figure 2.** (a) Acai seed, (b) Micronized Acai berry, (c) Micronized Acai berry at 100x magnification, (d) Micronized Acai berry at 2500x magnification, (e) NR/Acai surface 0 phr, (f) NR/Acai fracture 0 phr, (g) BN/Acai surface 10 phr, (h) NR/Acai fracture 10 phr, (i) NR/Acai surface 20 phr, (j) NR/Acai fracture 20 phr, (k) NR/Acai surface 30 phr, (l) NR/Acai fracture 30 phr, (m) NR/Acai surface 40 phr, (n) NR/Acai fracture 40 phr, (o) NR/Acai surface 50 phr and (p) NR/Acai fracture 50 phr phr.



**Figure 3.** (a1) SEM image of micronized acai, (a2) EDX of acai powder, (b1) SEM image of unfilled BN/Acai composite, (b2) EDX of unfilled NR/Acai composite, (c1) SEM image of the composite of NR/Acai 30 phr and (c2) EDX of the composite of NR/Acai 30 phr.

### 3.3. X-ray fluorescence analysis of micronized acai

Table 3 shows the values of the chemical composition of the acai residue determined by X-ray fluorescence testing. The data showed that the sample is mostly composed of carbon, minor alkali metals that enhance the action of accelerators (potassium, calcium, and rubidium), zinc which is used as an activating agent in the vulcanization process, and sulfur which is responsible for the formation of cross-links between the macromolecular chains of the rubber.

### 3.4. Elemental organic analysis (CHNOS) of micronized acai

The organic chemical composition by elemental analysis was performed to complement the XRF results and the values are shown in Table 4. The results obtained by the elemental analyzer show that the chemical elements present in the acai samples in larger quantities are carbon and oxygen, corroborating with the XRF results. The acai samples also showed significant amounts of hydrogen and sulfur.

**Table 3.** Chemical composition of acai residue by XRF.

Elements	Amounts (%)
<b>K</b>	1.293
<b>Si</b>	0.555
<b>P</b>	0.227
<b>S</b>	0.204
<b>Ca</b>	0.133
<b>Mn</b>	0.010
<b>Fe</b>	0.008
<b>Rb</b>	0.008
<b>Cu</b>	0.008
<b>Zn</b>	0.003
<b>CO<sub>2</sub></b>	97.551
<b>Total</b>	<b>100</b>

**Table 4.** Elemental chemical composition by elemental organic analysis.

Elements	Amounts (%)
C	42.33 ± 0.07
H	7.08 ± 0.04
N	0.73 ± 0.26
O	47.60 ± 0.28
S	2.27 ± 0.04
<b>Total</b>	<b>100</b>

### 3.5. Density, Hardness (Shore A) and Abrasion Loss

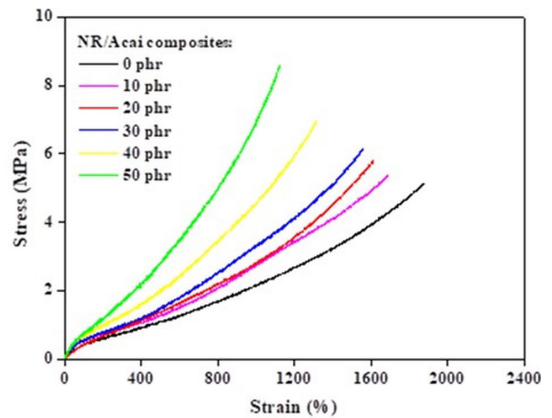
Table 5 presents the values of density, hardness on the Shore A scale, and the abrasion loss of NR/Acai composites. The density of the composites gradually increased with the incorporation of fillers ranging from 1 to 1.13 g cm<sup>-3</sup>. The hardness values also increased with the addition of fillers because the presence of fillers restricts the mobility of the molecular rubber chains resulting in the hardening of the composite. The acai waste was used without any chemical pre-treatment. The micronization reduced the particle size and generated mechanical reinforcement in the composite, increasing tensile strength due to a strong interfacial interaction with the matrix. On the other hand, the values of the abrasion loss presented an increase with the increase of the inserted filler. This behavior is due to the fiber length and its dispersion in the matrix. The fibrous nature of the filler was responsible for the formation of stress points in the matrix that favored mass loss during wear at the expense of friction. Another point was the generation of heat due to fiber-fiber interaction because of the large amount of filler present in the polymeric matrix.

### 3.6. Tensile strength at break analysis of composites and accelerated aging test

Figure 4 shows the stress-strain curves of the composites. The presence of the residue increased the stiffness of the material, decreasing the deformation and increasing the values of the tensile strength at break. This reinforcement is exclusively due to the adhesion between the acai residue and the rubber, requiring more tension for rupture<sup>25</sup>. The acai residues reinforced the tensile strength of the composite, and the reinforcement variations are related to the amount inserted and the dispersion of acai in the polymeric matrix. In the composites with 50 phr, the results were the most satisfactory compared to those with the lowest amount of acai residue. The increment in quantities of acai residues added contributed to the increase in tensile strength at break in all composites. This fact indicates that this amount of acai increases the acai/rubber interfacial adhesion, reinforcing the main chain and reducing the deformability of the polymer matrix. In composites, the form of a dispersion of the reinforcing agent, its dimensions, and the coupling agent greatly influence the final mechanical properties<sup>26</sup>. On the other hand, the form of dispersion or processing will also define the final dimensions of the fiber, reflected in its aspect ratio<sup>27</sup>. The classical model of micromechanics of reinforcement in polymeric composites stipulates that the

**Table 5.** Results of density, hardness (Shore A) and abrasion loss tests of NR/Acai composites.

Composites NR/Acai	Density (g cm <sup>-3</sup> )	Hardness (Shore A)	Abrasion loss (mm <sup>3</sup> (40 m) <sup>-1</sup> )
0 phr	1.01	46 ± 0	216 ± 7
10 phr	1.05	47 ± 1	283 ± 4
20 phr	1.07	50 ± 1	340 ± 17
30 phr	1.09	51 ± 0	340 ± 20
40 phr	1.11	53 ± 1	338 ± 10
50 phr	1.13	56 ± 0	354 ± 12

**Figure 4.** Stress-Strain curves of NR/Acai composites.

polymer-reinforcement interface is composed of a thin and rigid restricted layer, with perfect interfacial adhesion or high frictional forces between fiber and matrix, to ensure an efficient stress transfer<sup>28</sup>.

Table 6 presents the tensile strength results at break tests with aged and non-aged specimens.

When a rubber product is subjected to mechanical stress, certain mechanical properties are required in response to the stress required. Table 6 shows the modulus values at 300% elongation of the vulcanizates. With the insertion of the acai residue, a small reinforcement occurs. This reinforcement is a result of the crosslinking density, the good dispersion of the fillers in the polymeric matrix, and the interaction between filler/rubber. The results obtained by the Mooney-Rivlin and Lorenz-Park methods confirm this reinforcement promoted by the filler. The thermo-oxidative aging process caused a reduction in tensile strength and strain at break, probably resulting from the degradation of crosslinks. Table 6 shows that the unfilled composite was the one that was most influenced by thermo-oxidative degradation and that the presence of fillers mitigated the aging effects of the natural rubber compound.

### 3.7. Density of cross-links by swelling – Flory-Rehner

The crosslinking reactions are important for evaluating the general performance of the rubber. The analysis of the crosslinking densities provides relevant information, which can be used to improve the mechanical and thermal

**Table 6.** Results of tensile strength tests at the break with aged and non-aged NR/Acai composites samples.

Composites NR/Acai	Non-aged		Modulus 300%	Aged		Loss due to aging	
	Strain (%)	Stress (MPa)		Strain (%)	Stress (MPa)	Strain (%)	Stress (%)
0 phr	1871 ± 28	5.2 ± 0.7	0.8	767 ± 37	2.4 ± 0.8	59	54
10 phr	1691 ± 33	5.4 ± 0.3	0.87	710 ± 51	3.6 ± 0.6	58	33
20 phr	1615 ± 71	5.8 ± 0.9	1.08	775 ± 66	4 ± 0.8	52	31
30 phr	1553 ± 27	6.2 ± 0.4	1.14	931 ± 46	4.2 ± 0.5	40	32
40 phr	1321 ± 48	7 ± 0.8	1.38	872 ± 53	4.7 ± 0.7	34	33
50 phr	1117 ± 52	8.6 ± 0.4	1.82	793 ± 69	6.2 ± 0.9	29	28

properties of the composites<sup>29</sup>. The determination of crosslink densities using organic solvent until equilibrium swelling using the equation developed by Flory-Rehner gives good results<sup>30</sup>. Table 7 presents the crosslinking densities values by the Flory-Rehner methodology. According to Table 7, the crosslinking densities of the composites gradually increase with the addition of filler. These results confirm the strong interaction between the polymer matrix and the filler, as this interaction acts as a block for the penetration of the solvent into the polymer chain structure.

The solvent tends to penetrate the polymer more easily at interfaces that are parallel and perpendicular to the fiber, where the fiber-rubber interfacial interaction is relatively weak. On the other hand, the results obtained with the Lorentz – Park Method show a strong interaction between the fiber and the elastomer, this behavior indicates that the penetration of the solvent is difficult. In this way, the filler (fiber) behaves as a kind of cross-link, increasing the number of cross-links verified in the swelling tests. Similar behaviors are reported in the literature<sup>31-33</sup>.

### 3.8. Crosslink density – Mooney-Rivlin

The crosslinking densities were determined by the Mooney-Rivlin method from the results obtained in the tensile strength tests of the vulcanized NR/Acai composites. In Figure 5, linear regression curves were plotted to estimate the values of the constants  $C_1$  and  $C_2$  of the Mooney-Rivlin methodology.

Table 8 shows the values of the crosslink densities. The constant  $C_1$  values increase with increasing fillers on the composites. According to Rooj et al.<sup>34</sup>,  $C_1$  and  $C_2$  are related to the network structure and the flexibility of the network chains, respectively. Mooney-Rivlin curves showed an increment in the slope attributed to a lower elasticity of the chains due to the strong interaction between the polymer matrix and the filler<sup>35,36</sup>. The Mooney-Rivlin coefficients measured from the stress-strain curves (Table 8) confirm the strong interaction between the acai residue and the elastomeric matrix. Since, when subjected to a traction force, elastic deformation occurs proportional to the requested effort, after the limit of elastic deformation, plastic deformation occurs where the matrix and the filler act in synergy until the composite ruptures.

### 3.9. Analysis of interfacial interaction by the Lorenz-Parks method

The interfacial interaction between the filler and the matrix was determined by the equation of Lorenz and Parks. Figure 6 shows the variation curve  $Q_f/Q_g$  vs.  $e^{-z}$  of

**Table 7.** Density of crosslinks by swelling – Flory-Rehner method.

Composites NR/Acai	Flory-Rehner $v \times 10^{-4}(\text{mol cm}^{-3})$
0 phr	1.33
10 phr	1.59
20 phr	1.62
30 phr	1.72
40 phr	1.77
50 phr	1.97

**Table 8.** Crosslink density by the Mooney-Rivlin method.

Composites	Mooney-Rivlin		
	$\eta_x \cdot 10^{-4}$ ( $\text{mol cm}^{-3}$ )	$C_1$	$C_2$
0 phr	1.24	0.1537	0.3307
10 phr	1.41	0.1749	0.2828
20 phr	1.64	0.2028	0.0613
30 phr	1.90	0.2359	0.2962
40 phr	1.95	0.2420	0.0864
50 phr	2.65	0.3288	0.1961

NR composites with acai residues and gum without filler (reference sample). Parameters a and b were constant, with numerical values of 0.7538 and 0.2721, respectively, and correlation coefficient R equal to 0.9. According to Lorentz and Park, values of the “a” constant greater than 0.7 indicate a strong interaction between the acai fibers and the rubber matrix. Santos et al.<sup>22</sup> obtained similar “a” and “b” constants values for compounds obtained from natural rubber with leather residue.

Figure 7 shows the reduction of the values decreasing as increase the amount of fiber added, and this behavior confirms the beneficial interaction between the filler and the matrix.

### 3.10. Infrared spectroscopic analysis with Fourier transformed in ATR mode

Figure 8 shows the FTIR spectra of acai powder residues and NR/Acai composites, and Table 9 lists the major bands. The acai power spectrum shows a broad band in the 3640-3020  $\text{cm}^{-1}$  range, which we attribute to cellulose and lignin O–H stretching<sup>5,9</sup>. The presence of water in the acai samples can be assumed based on the characteristic O–H stretching of the water molecule, which became almost undetectable in the spectra of the composite materials after



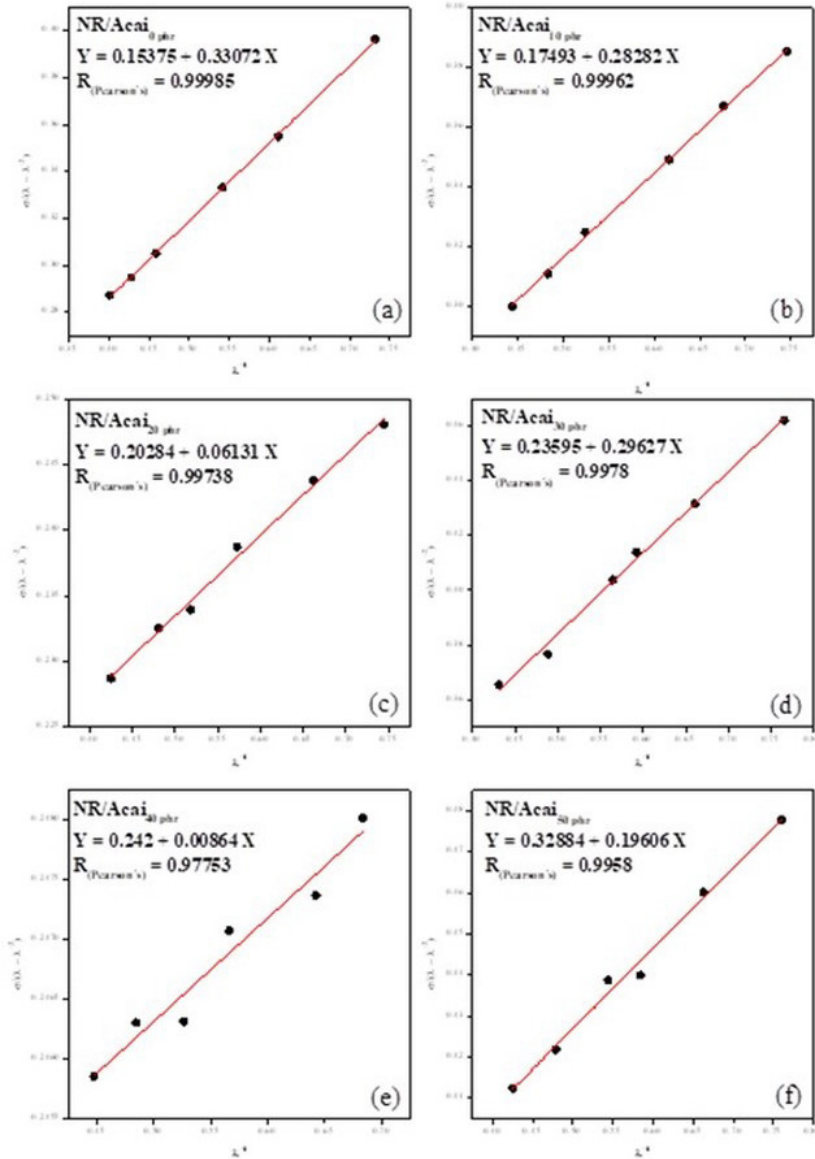


Figure 5. Plotting of  $\sigma/(\lambda - \lambda^2)$  versus  $\lambda^1$  of NR/Acai composites with (a) 0 phr, (b) 10 phr, (c) 20 phr, (d) 30 phr, (e) 40 phr and (f) 50 phr.

vulcanization. This observation is consistent with the fact that the composites underwent vulcanization at 150 °C, a temperature higher than the boiling point of water, and corroborates the TG analysis results. The band absorption at 2933  $\text{cm}^{-1}$  is associated with C–H stretching of methyl and methylene groups of cellulose. The 1730  $\text{cm}^{-1}$  band is associated with C=O carboxyl groups from hemicellulose and lignin and the 1640  $\text{cm}^{-1}$  band is associated with C=O stretching of aromatic skeletal of lignin<sup>9,37</sup>.

The spectrum of vulcanized NR without acai powder (0 phr) showed three peaks at wavelength intervals of 2852–2960  $\text{cm}^{-1}$ , suggesting functional group vibrations of the NR structure. As reported in the literature<sup>39,40</sup>, the peaks at 2960  $\text{cm}^{-1}$ , 2918  $\text{cm}^{-1}$  and 2852  $\text{cm}^{-1}$  correspond to the stretching vibrations of the  $-\text{CH}_3$ ,  $-\text{CH}_2$ , and  $-\text{CH}$  groups, respectively. The absorption bands at 1662  $\text{cm}^{-1}$  attributed to

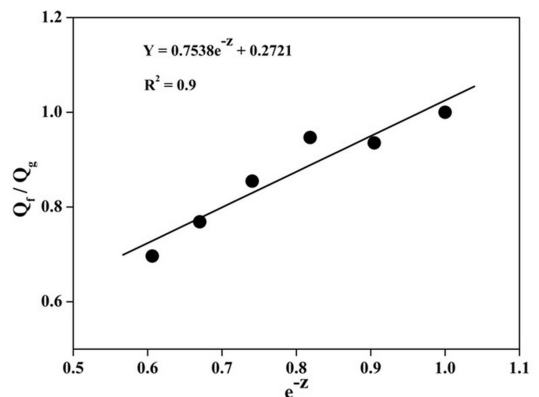
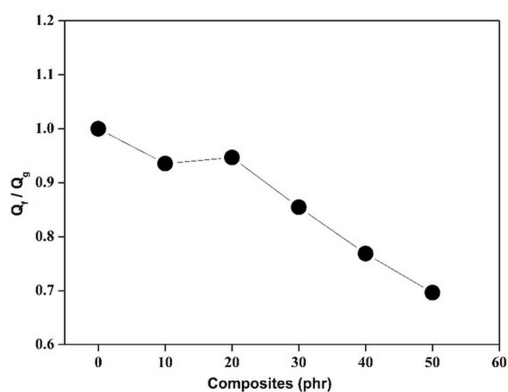


Figure 6. Variation curve  $Q_1/Q_g$  vs.  $e^{-Z}$  of NR composites with acai residues and gum without filler (reference sample).

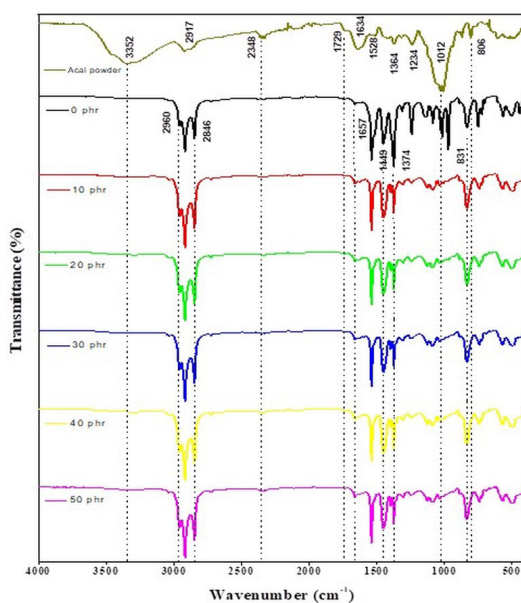
**Table 9.** FTIR spectra bands of micronized acai and NR/Acai composites.

Micronized acai residues			
Wavenumber (cm <sup>-1</sup> )	Assignments	Components	Ref.
3640 - 3020	-OH stretching	Cellulose and lignin	5,9
2933	C-H stretching of methyl and methylene groups	Cellulose	5
1730	C=O stretching of carboxyl groups of lignin or groups of hemicelluloses	Lignin or hemicellulose	5,9,37
1640	C=O stretching (aromatic skeletal vibration)	Lignin	9,37
1430	C-H deformation (methyl and methylene)	Lignin	9,37
1378	Stretching vibrations of different carbohydrate groups	---	5
1242	C-O stretching vibration (acetyl groups)	Lignin and hemicellulose	5,9
1031	C-O deformation asymmetric in the primary alcohol from guaiacyl	---	37,38
Natural Rubber			
Wavenumber (cm <sup>-1</sup> )	Assignments	Components	Ref.
2960	-CH <sub>3</sub> stretching vibration	Isoprene	39-41
2918	-CH <sub>2</sub> stretching vibration	Isoprene	9
2852	-CH stretching vibration	Isoprene	39-41
1662	C=C stretching vibration	Isoprene	39,40,42
1450	-CH <sub>3</sub> bending vibration	Isoprene	39,40
1374	-CH <sub>2</sub> bending vibration	Isoprene	39,40

**Figure 7.** Effect of the filler on Q<sub>f</sub>/Q<sub>g</sub> of NR composites with acai fibers and gum.

C=C stretching vibration, 1450 cm<sup>-1</sup> attributed to -CH<sub>3</sub> bending vibration, and 1374 cm<sup>-1</sup> attributed to -CH<sub>2</sub> bending vibration suggest that the structure of NR remained unchanged even after the process of incorporating acai residues.

When we examined the spectra of the composites from 0 to 50 phr, we found no significant changes in the absorption bands with the increase of the acai residues in the polymeric matrix. This fact reinforces that acai residue addition does not affect the chemical structure of natural rubber. In the study by Datta et al.<sup>43</sup>, the authors did not observe an increase in the intensity of the characteristic peaks with an increase in the

**Figure 8.** FTIR spectra of acai powder and NR/Acai composites.

amount of lignin in the composites. Datta et al.<sup>43</sup> attributed this behavior to the formation of lignin clusters, which occurred as the amount of lignin increased.

Table 9 identifies the spectra of the compounds.

### 3.11. Thermogravimetric Analysis (TG)

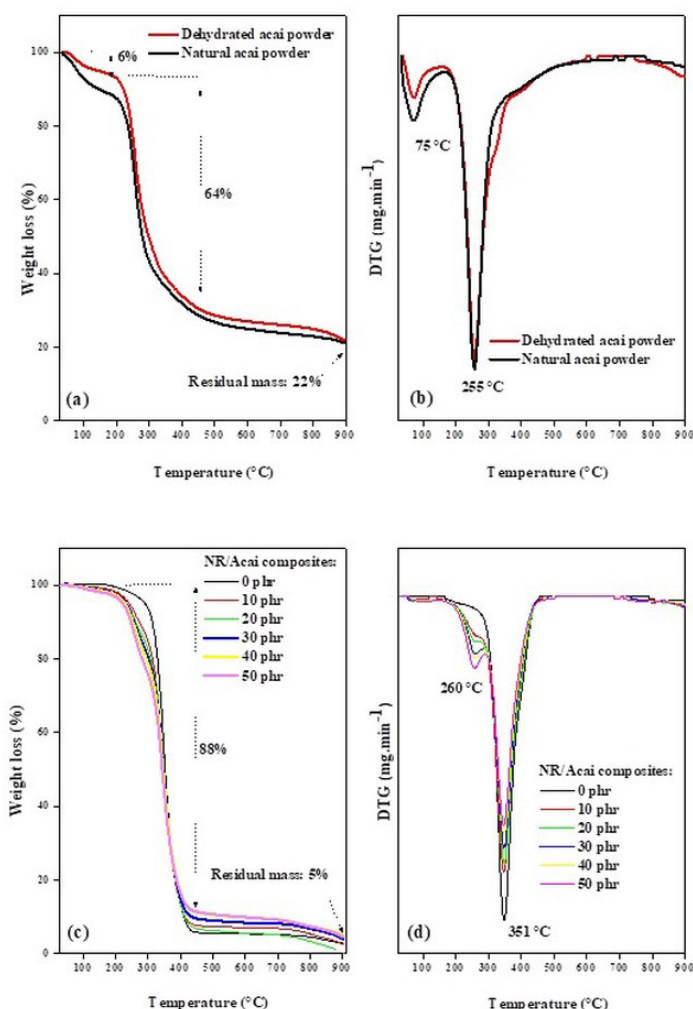
The thermal stability of the composites was investigated by thermogravimetric analysis. Figure 9a shows the mass loss curve of acai in natura form and after the drying process. The degradation of this material occurs in two stages: the first stage occurs between 50 °C and 200 °C with a mass loss of 6%, attributed to the outflow of adsorbed water in the fiber. The second stage, with a mass loss of 64% between 200 °C and 450 °C, refers to the degradation of hemicellulose, cellulose, and lignin. The residual mass is approximately 22% attributed to inorganic materials of the sample, such as iron, potassium, calcium, and rubidium, identified in the X-ray fluorescence analysis. In the biomass derivative curve shown in Figure 9b, we observed two events of greater intensity, the first referring to the evaporation of the moisture contained in the material in the temperature range of 75 °C and the second at 255 °C linked to the dehydration reactions of the (–OH) groups from the polysaccharides lignocellulosic<sup>44</sup>.

Figure 9c shows the mass loss curves of the NR/Acai composites. Between 50 °C and 450 °C, the composites

had a significant mass loss of 88%, which was attributed to the decomposition of the hemicellulose and the cellulose bonds breaking. All composites showed about 5% residual mass. Figure 9d presents the DTG of the composites, and four main events were observed. The first, around 69 °C, is associated with the loss of absorbed water in acai residues. The second event is at 260 °C and refers to the decomposition of hemicellulose and cellulose. The third event at 296 °C is due to lignin decomposition. And the last event, at 351 °C, is related to the degradation of the main structure of natural rubber, isoprene. According to Martins et al.<sup>45</sup>, such behaviors indicate characteristics like those of other fibers added into the polymeric matrix, suggesting that acai fibers can be processed by vulcanization.

## 4. Application

Paiva et al.<sup>46</sup> produced sandals using natural rubber composites with sugarcane bagasse fibers, reporting the requirements for the application of composites as soles raw material for the footwear industry, being a minimum



**Figure 9.** Curves of (a) TG of micronized in natura and dehydrated acai, (b) DTG of micronized in natura and dehydrated acai, (c) TG of NR/Acai composites and (d) DTG of NR/Acai composites.

of 55 shore A of hardness, maximum of 400 mm<sup>3</sup>·40 m<sup>-1</sup> of abrasion loss, a minimum of 5 MPa of stress and minimum of 200% of elongation at break. The composites of rubber with 50 phr of Acai reach 56 shore A of hardness, 8.6 MPa of stress at break or even 6.2 MPa after aging, elongation average of 1117% (793% after aging), and 354 mm<sup>3</sup>·40 m<sup>-1</sup> of abrasion loss, satisfying all requirements.

## 5. Conclusion

This work showed the possibility of recycling the micronized acai residue to produce new composites based on a polymeric matrix. The rheometric parameters showed that the presence of filler significantly reduces the vulcanization time. The cross-link density increased with the addition of the filler, as shown by the results obtained by Flory-Rehner and Mooney-Rivlin methodologies. The interaction studies between the polymeric matrix and the filler applying the Lorenz-Parks model showed a strong interaction between the natural rubber and the acai residue, justifying the mechanical reinforcement. The thermal behavior of the polymeric matrix was altered due to the degradation processes of hemicellulose, cellulose, and lignin. Infrared spectroscopy revealed no chemical interaction between the matrix and the filler. Thus, this paper demonstrates the possibility of reusing acai waste as a sustainable raw material for biocomposite production and generating added value to the acai biomass waste contributing to environmental conservation.

## 6. Acknowledgements

The authors would like to thank the Fundação de Amparo à Pesquisa do Estado de São Paulo (FAPESP) for the financial support under grant n° 2016/03208-0 and POSMAT-CAPES-PROEX for the student assistance.

## 7. References

- Lima ACP, Bastos DLR. Physicochemical characterization of residual biomass (seed and fiber) from açai (*Euterpe oleracea*) processing and assessment of the potential for energy production and bioproducts. *Biomass Convers Biorefin.* 2021;11(3):925-35. <http://dx.doi.org/10.1007/s13399-019-00551-w>.
- Barbosa AM, Santos GM, Melo GMM, Litaiff HA, Martorano LG, Giaccon VM. Evaluation of the use of açai seed residue as reinforcement in polymeric composite. *Polym Polymer Compos.* 2022;30:09673911221108307.
- Martins MA, Pessoa JDC, Gonçalves PS, Souza FI, Mattoso LHC. Thermal and mechanical properties of the açai fiber/natural rubber composites. *J Mater Sci.* 2008;43(19):6531-8. <http://dx.doi.org/10.1007/s10853-008-2842-4>.
- Okolie JA, Nanda S, Dalai AK, Kozinski JA. Chemistry and specialty industrial applications of lignocellulosic biomass. *Waste Biomass Valoriz.* 2021;12(5):2145-69. <http://dx.doi.org/10.1007/s12649-020-01123-0>.
- Azevedo A, de Matos P, Marvila M, Sakata R, Silvestro L, Gleize P, et al. Rheology, hydration, and microstructure of portland cement pastes produced with ground açai fibers. *Appl Sci (Basel).* 2021;11(7):3036. <http://dx.doi.org/10.3390/app11073036>.
- Oliveira BP, Balieiro LCS. Eco-friendly polyurethane foams based on castor polyol reinforced with açai residues for building insulation. *J Mater Cycles Waste Manag.* 2022;24(2):553-68. <http://dx.doi.org/10.1007/s10163-021-01341-1>.
- Teixeira JN, Silva DW, Vilela AP, Savastano Junior H, de Siqueira Brandão Vaz LEV, Mendes RF. Lignocellulosic materials for fiber cement production. *Waste Biomass Valoriz.* 2020;11(5):2193-200. <http://dx.doi.org/10.1007/s12649-018-0536-y>.
- Núñez-Decap M, Wechsler-Pizarro A, Vidal-Vega M. Mechanical, physical, thermal and morphological properties of polypropylene composite materials developed with particles of peach and cherry stones. *Sustain Mater Technol.* 2021;29:e00300. <http://dx.doi.org/10.1016/j.susmat.2021.e00300>.
- Tavares FFC, Almeida MDC, Silva JAP, Araújo LL, Cardozo NSM, Santana RMC. Thermal treatment of açai (*Euterpe oleracea*) fiber for composite reinforcement. *Polímeros.* 2020;30(1):e2020003. <http://dx.doi.org/10.1590/0104-1428.09819>.
- ASTM: American Society for Testing and Materials. ASTM D3182-21a: standard practice for rubber—materials, equipment, and procedures for mixing standard compounds and preparing standard vulcanized sheets. West Conshohocken: ASTM; 2021.
- ASTM: American Society for Testing and Materials. ASTM D2084-19a: standard test method for rubber property—vulcanization using oscillating disk cure meter. West Conshohocken: ASTM; 2019.
- ASTM: American Society for Testing and Materials. ASTM D297-21: standard test methods for rubber products—chemical analysis. West Conshohocken: ASTM; 2022.
- Flory PJ, Rehner J Jr. Statistical mechanics of cross-linked polymer networks I. Rubberlike elasticity. *J Chem Phys.* 1943;11(11):512-20. <http://dx.doi.org/10.1063/1.1723791>.
- Mooney M. A theory of large elastic deformation. *J Appl Phys.* 1940;11(9):582-92. <http://dx.doi.org/10.1063/1.1712836>.
- Gruendken M, Koda D, Dryzek J, Blume A. Low molecular weight 'liquid' polymer extended compounds, impact on free volume and crosslink density studied by positron lifetime spectroscopy and stress-strain analysis according to Mooney-Rivlin. *Polym Test.* 2021;100:107239. <http://dx.doi.org/10.1016/j.polymertesting.2021.107239>.
- Sombatsompop N. Practical use of the Mooney-Rivlin equation for determination of degree of crosslinking of swollen nr vulcanisates. *Sci Asia.* 1998;24(3):199-204. <http://dx.doi.org/10.2306/scienceasia1513-1874.1998.24.199>.
- ASTM: American Society for Testing and Materials. ASTM D412-16: standard test methods for vulcanized rubber and thermoplastic elastomers—tension. West Conshohocken: ASTM; 2021.
- ASTM: American Society for Testing and Materials. ASTM D573-04: standard test method for rubber – deterioration in an air oven. West Conshohocken: ASTM; 2019.
- ASTM: American Society for Testing and Materials. ASTM D2240-15: standard test method for rubber property—durometer hardness. West Conshohocken: ASTM; 2021.
- ASTM: American Society for Testing and Materials. ASTM D5963-04: standard test method for rubber property—abrasion resistance (rotary drum abrader). West Conshohocken: ASTM; 2019.
- Lorenz O, Park CR. The crosslinking efficiency of some vulcanizing agents in natural rubber. *Journal of Polymer Science.* 1961;50(154):299-312. <http://dx.doi.org/10.1002/pol.1961.1205015404>.
- Santos RJ, Hiranobe CT, Dognani G, Silva MJ, Paim LL, Cabrera FC, et al. Using the Lorenz–Park, Mooney–Rivlin, and dynamic mechanical analysis relationship on natural rubber/leather shavings composites. *J Appl Polym Sci.* 2022;139(14):51880. <http://dx.doi.org/10.1002/app.51880>.
- ASTM: American Society for Testing and Materials. ASTM D6370-99: standard test method for rubber—compositional analysis by thermogravimetry (TGA). West Conshohocken: ASTM; 2019.
- Melo PS, Selani MM, Gonçalves RH, Paulino JO, Massarioli AP, Alencar SM. Açai seeds: an unexplored agro-industrial

- residue as a potential source of lipids, fibers, and antioxidant phenolic compounds. *Ind Crops Prod.* 2021;161:113204. <http://dx.doi.org/10.1016/j.indcrop.2020.113204>.
25. Rattanasom N, Prasertsri S, Ruangritnumchai T. Comparison of the mechanical properties at similar hardness level of natural rubber filled with various reinforcing-fillers. *Polym Test.* 2009;28(1):8-12. <http://dx.doi.org/10.1016/j.polymertesting.2008.08.004>.
  26. Rabello M. *Adivisão de polímeros*. São Paulo: Artliber; 2000.
  27. Mano B, Araújo JR, Spinacé MAS, De Paoli M-A. Polyolefin composites with curaua fibres: effect of the processing conditions on mechanical properties, morphology and fibres dimensions. *Compos Sci Technol.* 2010;70(1):29-35. <http://dx.doi.org/10.1016/j.compscitech.2009.09.002>.
  28. Plueddemann EP. *Silane coupling agents*. New York: Plenum Press; 1991. p. 79-151. [http://dx.doi.org/10.1007/978-1-4899-2070-6\\_4](http://dx.doi.org/10.1007/978-1-4899-2070-6_4).
  29. Kim DY, Park JW, Lee DY, Seo KH. Correlation between the crosslink characteristics and mechanical properties of natural rubber compound via accelerators and reinforcement. *Polymers (Basel)*. 2020;12(9):2020. <http://dx.doi.org/10.3390/polym12092020>.
  30. Hiranobe CT, Ribeiro GD, Torres GB, Reis EAP, Cabrera FC, Job AE, et al. Cross-linked density determination of natural rubber compounds by different analytical techniques. *Mater Res.* 2021;24(suppl 1):e20210041. <http://dx.doi.org/10.1590/1980-5373-mr-2021-0041>.
  31. Varghese S, Kuriakose B, Thomas S, Joseph K. Effect of adhesion on the equilibrium swelling of short sisal fiber reinforced natural rubber composites. *Rubber Chem Technol.* 1995;68(1):37-49. <http://dx.doi.org/10.5254/1.3538730>.
  32. Coran AY, Boustany K, Hamed P. Unidirectional fiber-polymer composites: swelling and modulus anisotropy. *J Appl Polym Sci.* 1971;15(10):2471-85. <http://dx.doi.org/10.1002/app.1971.070151014>.
  33. Jacob M, Thomas S, Varughese KT. Mechanical properties of sisal/oil palm hybrid fiber reinforced natural rubber composites. *Compos Sci Technol.* 2004;64(7-8):955-65. [http://dx.doi.org/10.1016/S0266-3538\(03\)00261-6](http://dx.doi.org/10.1016/S0266-3538(03)00261-6).
  34. Rooj S, Das A, Heinrich G. Tube-like natural halloysite/fluoroelastomer nanocomposites with simultaneous enhanced mechanical, dynamic mechanical and thermal properties. *Eur Polym J.* 2011;47(9):1746-55. <http://dx.doi.org/10.1016/j.eurpolymj.2011.06.007>.
  35. Schieppati J, Schritteser B, Wondracek A, Robin S, Holzner A, Pinter G. Temperature impact on the mechanical and fatigue behavior of a non-crystallizing rubber. *Int J Fatigue.* 2021;144:106050. <http://dx.doi.org/10.1016/j.ijfatigue.2020.106050>.
  36. He S, Hu J, Zhang C, Wang J, Chen L, Bian X, et al. Performance improvement in nano-alumina filled silicone rubber composites by using vinyl tri-methoxysilane. *Polym Test.* 2018;67:295-301. <http://dx.doi.org/10.1016/j.polymertesting.2018.03.023>.
  37. Martins LS, Silva NGS, Claro AM, Amaral NC, Barud HS, Mulinari DR. Insight on açai seed biomass economy and waste cooking oil: eco-sorbent castor oil-based. *J Environ Manage.* 2021;293:112803. <http://dx.doi.org/10.1016/j.jenvman.2021.112803>.
  38. Kubo S, Kadla JF. Hydrogen bonding in lignin: a Fourier transform infrared model compound study. *Biomacromolecules.* 2005;6(5):2815-21. <http://dx.doi.org/10.1021/bm050288q>.
  39. Rosli NA, Ahmad I, Anuar FH, Abdullah I. Mechanical and thermal properties of natural rubber-modified poly (lactic acid) compatibilized with telechelic liquid natural rubber. *Polym Test.* 2016;54:196-202. <http://dx.doi.org/10.1016/j.polymertesting.2016.07.021>.
  40. Manohar N, Jayaramudu J, Suchishmita S, Rajkumar K, Babul Reddy A, Sadiku ER, et al. A unique application of the second order derivative of FTIR-ATR spectra for compositional analyses of natural rubber and polychloroprene rubber and their blends. *Polym Test.* 2017;62:447-53. <http://dx.doi.org/10.1016/j.polymertesting.2017.07.030>.
  41. Agrebi F, Ghorbel N, Bresson S, Abbas O, Kallel A. Study of nanocomposites based on cellulose nanoparticles and natural rubber latex by ATR/FTIR spectroscopy: the impact of reinforcement. *Polym Compos.* 2019;40(5):2076-87. <http://dx.doi.org/10.1002/pc.24989>.
  42. Rolere S, Liengprayoon S, Vaysse L, Sainte-Beuve J, Bonfils F. Investigating natural rubber composition with Fourier Transform Infrared (FT-IR) spectroscopy: a rapid and non-destructive method to determine both protein and lipid contents simultaneously. *Polym Test.* 2015;43:83-93. <http://dx.doi.org/10.1016/j.polymertesting.2015.02.011>.
  43. Datta J, Parcheta P, Surówka J. Softwood-lignin/natural rubber composites containing novel plasticizing agent: preparation and characterization. *Ind Crops Prod.* 2017;95:675-85. <http://dx.doi.org/10.1016/j.indcrop.2016.11.036>.
  44. Ibanez PG, Sanchez M, Cabanillas A. Thermogravimetric analysis of olive-oil residue in air atmosphere. *Fuel Process Technol.* 2006;87(2):103-7. <http://dx.doi.org/10.1016/j.fuproc.2005.08.005>.
  45. Martins MA, Mattoso LHC, Pessoa JDC. Comportamento térmico e caracterização morfológica das fibras de mesocarpo e caroço do açai (*Euterpe oleracea* Mart.). *Rev Bras Frutic.* 2009;31(4):1150-7. <http://dx.doi.org/10.1590/S0100-29452009000400032>.
  46. Paiva FFG, Maria VPK, Torres GB, Dognani G, Santos RJ, Cabrera FC, et al. Sugarcane bagasse fiber as semi-reinforcement filler in natural rubber composite sandals. *J Mater Cycles Waste Manag.* 2019;21(2):326-35. <http://dx.doi.org/10.1007/s10163-018-0801-y>.